



Universidade de São Paulo

Biblioteca Digital da Produção Intelectual - BDPI

Departamento de Física e Ciências Materiais - IFSC/FCM

Artigos e Materiais de Revistas Científicas - IFSC/FCM

2014-11

Atomic lighthouse effect

Journal of the Optical Society of America A, Washington, DC : Optical Society of America - OSA, v. 31, n. 11, p. 2511-2517, Nov. 2014
<http://www.producao.usp.br/handle/BDPI/50550>

Downloaded from: Biblioteca Digital da Produção Intelectual - BDPI, Universidade de São Paulo

Atomic lighthouse effect

C. E. Máximo,^{1,*} R. Kaiser,² Ph. W. Courteille,¹ and R. Bachelard¹

¹*Instituto de Física de São Carlos, Universidade de São Paulo, 13560-970 São Carlos, SP, Brazil*

²*Université de Nice Sophia Antipolis, CNRS, Institut Non-Linéaire de Nice, UMR 7335, F-06560 Valbonne, France*

*Corresponding author: dumax1@gmail.com

Received July 29, 2014; revised September 22, 2014; accepted September 22, 2014;
posted September 23, 2014 (Doc. ID 219885); published October 27, 2014

We investigate the deflection of light by a cold atomic cloud when the light–matter interaction is locally tuned via the Zeeman effect using magnetic field gradients. This “lighthouse” effect is strongest in the single-scattering regime, where deviation of the incident field is largest. For optically dense samples, the deviation is reduced by collective effects, as the increase in linewidth leads to a decrease in magnetic field efficiency. © 2014 Optical Society of America

OCIS codes: (020.0020) Atomic and molecular physics; (020.1670) Coherent optical effects; (020.7490) Zeeman effect; (290.4210) Multiple scattering.
<http://dx.doi.org/10.1364/JOSAA.31.002511>

1. INTRODUCTION

The interference of light scattered by different particles of an ensemble is at the origin of a variety of collective phenomena such as superradiance [1], Bragg scattering, or collective frequency shifts [2–4]. The phenomena can be classified in two distinct regimes according to whether the scatterers interact with each other via mediation of the incident light or not. Bragg scattering, for example, is the result of a far-field interference of the light waves scattered by an optically dilute, periodic structure. In this case, even in the absence of communication between the scatterers, the radiated light pattern provides information on the scattering structure, a fact that is extensively used, e.g., in crystallography. On the other hand, optically dense structures lead to multiple scattering and strong interference in the near-field (i.e., within the structure) between the light waves scattered from different particles. One example is the opening of photonic bandgaps in period structures [5–9].

Cold atomic clouds are particularly attractive experimentation platforms as powerful techniques not only to shape the density distribution but also to fine-tune the light–matter interaction over wide ranges. Here, we show that sufficiently cold atomic clouds exposed to a gradient of the strength of the light–matter interaction deflect light due to collective scattering in the single-scattering regime. We propose to implement the required gradient by an inhomogeneous magnetic field exploiting the Zeeman effect. Because this phenomenon is reminiscent of an effect studied in nuclear physics called the “lighthouse effect” [10–13], we call this effect the “atomic lighthouse effect.”

The nuclear lighthouse effect was used to perform spectroscopy and the transformation from time to angular coordinates allowed us to detect timescales difficult to achieve with present detection schemes. Similar light deviation effects have been experimentally observed for light passing through an atomic vapor in slow light and electromagnetically induced transparency schemes using either magnetically [14,15] or optically induced gradients [16,17].

We will show in this paper that the atomic lighthouse effect can be obtained on a two-level scheme and is a result of the interference of the light radiated by independent atoms. Similar to Bragg scattering, it is thus fully determined by the single-photon structure factor of the atomic cloud. However, light-induced interatomic cooperation dramatically *alters* the lighthouse effect in the case of optically dense samples. We prove this via calculations and simulations accounting for the light-induced interactions between the atoms in the multiple-scattering regime. The alteration can be understood as an increase in the atomic linewidth, due to the atoms’ cooperation, that reduces the Zeeman effect. Hence, the reduction of the lighthouse effect provides a direct signature of cooperativity.

2. COUPLED DIPOLE MODEL

We describe the light deviation by a cloud of atoms with a model treating all atomic dipoles as being coupled via the incident light. This allows us to account for interferences between these dipoles in the optically dense regime. Photon random walk approaches are not sufficient. Furthermore, all dipoles are exposed to a locally varying atom–light interaction inducing an inhomogeneous phase profile of the dipole excitation across the atomic cloud.

Let us start by considering an ensemble of N two-level (g and e) atoms, each at a position \mathbf{r}_j ($j = 1, 2, \dots, N$), driven by a uniform laser beam with wave vector $\mathbf{k}_0 = k_0 \hat{\mathbf{z}}$. The detuning of the light from the atomic resonance is $\Delta_0 = \omega_0 - \omega_a$, and the Rabi frequency is $\Omega_0 = dE_0/\hbar$, where d is the dipole matrix element, E_0 is the field amplitude, and \hbar is the Planck constant. The atom–light interaction is locally tuned with an inhomogeneous magnetic field in the quantization direction $\mathbf{B}(\mathbf{r}_j) = \hat{\mathbf{z}}B(\mathbf{r}_j)$ (see Fig. 1).

Let us consider an electronic transition with a structureless ground state and single excited state Zeeman level. This system is described by the following Hamiltonian [18] in the rotating wave approximation:

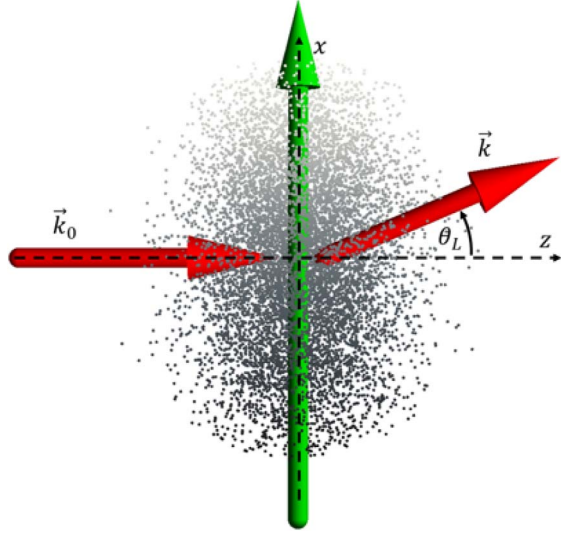


Fig. 1. Scheme of the atomic lighthouse effect. An incident laser beam labeled by its wave vector, \mathbf{k}_0 , is scattered from a cloud of cold atoms to which a transverse magnetic field gradient, ∇B , is applied. As a consequence, the light is deviated by an angle θ_L .

$$\begin{aligned} \hat{H} = & \frac{\hbar\Omega_0}{2} \sum_{j=1}^N (\hat{\sigma}_-^{(j)} e^{i\Delta_0 t - i\mathbf{k}_0 \cdot \mathbf{r}_j} + \text{h.c.}) \\ & + \hbar \sum_{j=1}^N \sum_{\mathbf{k}} g_{\mathbf{k}} (\hat{\sigma}_-^{(j)} \hat{a}_{\mathbf{k}}^\dagger e^{i\Delta_{\mathbf{k}} t - i\mathbf{k} \cdot \mathbf{r}_j} + \text{h.c.}) \\ & - \frac{\hbar}{2} \sum_{j=1}^N \Delta(\mathbf{r}_j) \sigma_z^{(j)}. \end{aligned} \quad (1)$$

$\Delta_{\mathbf{k}} = \omega_{\mathbf{k}} - \omega_a$ is the detuning between the field emitted into mode \mathbf{k} and the atomic transition ω_a . $g_{\mathbf{k}} = d\sqrt{\omega_{\mathbf{k}}/\hbar\epsilon_0 V_{\nu}}$ is the single-photon Rabi frequency for a photon volume V_{ν} . $\Delta(\mathbf{r}_j) = \mu_B m_j B(\mathbf{r}_j)/\hbar$ describes the (inhomogeneous) Zeeman effect, $\hat{\sigma}_-^{(j)} = |g_j\rangle\langle e_j|$ and $\hat{\sigma}_z^{(j)} = |e_j\rangle\langle e_j| - |g_j\rangle\langle g_j|$ are the Pauli matrices describing the de-excitation and the excited state population of atom j , respectively, whereas $\hat{a}_{\mathbf{k}}$ describes the photon annihilation in the mode \mathbf{k} . Note that the above model describes scalar light, an approximation valid for low density of atoms.

Under the Markov approximation and neglecting recoil or inelastic scattering, in the linear optics regime a scattering equation for the dipole excitation β_j can be derived (see, e.g., Ref. [2])

$$\begin{aligned} \frac{d\beta_j}{dt} = & \left[i(\Delta(\mathbf{r}_j) + \Delta_0) - \frac{\Gamma}{2} \right] \beta_j - \frac{i\Omega_0}{2} e^{i\mathbf{k}_0 \cdot \mathbf{r}_j} \\ & - \frac{\Gamma}{2} \sum_{m \neq j} \frac{\exp(i\mathbf{k}_0 \cdot (\mathbf{r}_j - \mathbf{r}_m))}{i\mathbf{k}_0 \cdot (\mathbf{r}_j - \mathbf{r}_m)} \beta_m, \end{aligned} \quad (2)$$

where $\Gamma = V_{\nu} g_{\mathbf{k}_0}^2 k_0^2 / \pi c$ is the transition linewidth, and $|\beta_j|^2$ corresponds to the probability for atom j to be excited. Since the laser Δ_0 is equivalent to a magnetic field offset, under the assumption of a single excited state Zeeman level, we may set $\Delta_0 = 0$ without loss of generality.

As the lighthouse effect relies on a global phase contrast in the dipole field rather than on disorder effects, we adopt a fluid description of the system introducing the local density

$\rho(\mathbf{r})$ and dipole field $\beta(\mathbf{r})$. Then, in the steady state regime, Eq. (2) turns into a Fredholm equation of the second type,

$$\beta(\mathbf{r}) = \beta^{(1)}(\mathbf{r}) + \int d^3\mathbf{r}' \rho(\mathbf{r}') K(\mathbf{r}, \mathbf{r}') \beta(\mathbf{r}'), \quad (3)$$

where we have introduced the single-scattering dipole excitation,

$$\beta^{(1)}(\mathbf{r}) = \frac{\Omega_0}{\Gamma} \frac{e^{i\mathbf{k}_0 \cdot \mathbf{r}}}{i + 2\Delta(\mathbf{r})/\Gamma}, \quad (4)$$

and the scattering kernel,

$$K(\mathbf{r}, \mathbf{r}') = \frac{1}{2i\Delta(\mathbf{r})/\Gamma - 1} \frac{e^{i\mathbf{k}_0 \cdot (\mathbf{r} - \mathbf{r}')}}{ik_0 |\mathbf{r} - \mathbf{r}'|}. \quad (5)$$

The consequence of a differential Zeeman effect is intuitive in the single-scattering limit Eq. (4), where the field $\Delta(\mathbf{r})$ modulates spatially the phase (and amplitude) of the dipole field, thus modifying the direction of superradiant emission of the cloud. In the multiple-scattering regime, a more detailed study must be performed in order to understand how the rescattering of the photons alters this new phase profile (see Section 4).

3. SINGLE-SCATTERING REGIME

For the sake of simplicity, we focus on a constant magnetic field gradient, which is orthogonal to the laser beam and cancels at the cloud's center: $B(\mathbf{r}) = \eta x$. We found the lighthouse effect to be strongest in this geometry. Indeed, for a central detuning $\Delta(\mathbf{r} = \mathbf{0})$ much larger than the one created by the gradient of the magnetic field bR (R the cloud radius), the resulting gradient of phase is tuned down by a factor $1/(1 + 4\Delta(\mathbf{0})^2/\Gamma^2)$, thus reducing the deflection angle.

We describe the cloud's density distribution by Gaussian spheres, which presents the analytical advantage of having a factorizable density in Cartesian coordinates:

$$\rho(x, y, z) = \frac{N}{(2\pi)^{3/2} R^3} e^{-\frac{x^2 + y^2 + z^2}{2R^2}}. \quad (6)$$

The far-field radiated electric field is given by

$$E(\mathbf{k}) = \frac{\hbar\Gamma}{id} \frac{e^{i\mathbf{k}_0 \cdot \mathbf{r}}}{r} \int d^3\mathbf{r}' \rho(\mathbf{r}') \beta(\mathbf{r}') e^{-i\mathbf{k} \cdot \mathbf{r}'}, \quad (7)$$

where, for clarity, we have omitted the time-dependent oscillating term $e^{-i\mathbf{k}_0 \cdot \mathbf{r}'}$. The field resulting from single-scattering $E^{(1)}$ is then calculated by replacing the complete dipole excitation β in Eq. (7) by the single-scattering excitation $\beta^{(1)}$ [see Eq. (4)]. For a Gaussian cloud, introducing the normalized gradient $\alpha = 2\mu_B \eta / (\hbar k_0 \Gamma)$ and the normalized cloud size $\sigma = k_0 R$, it reads (see Appendix A)

$$\begin{aligned} E^{(1)}(\mathbf{k}) = & -\sqrt{\frac{\pi N E_0}{2}} \frac{e^{i\mathbf{k}_0 \cdot \mathbf{r}}}{|\alpha| \sigma} \frac{1}{r} \exp\left(\frac{1}{2\alpha^2 \sigma^2} + \frac{\sin \theta}{\alpha} - \frac{\sigma^2}{2} (1 - \cos \theta)^2\right) \\ & \times \text{erfc}\left(\frac{1}{|\alpha| \sigma \sqrt{2}} + \frac{\text{sign}(\alpha) \sigma \sin \theta}{\sqrt{2}}\right), \end{aligned} \quad (8)$$

with $\alpha \neq 0$, $\phi = 0$, and $0 \leq \theta \leq 2\pi$. As can be seen in Fig. 3, this formula describes very well the scattering process in the

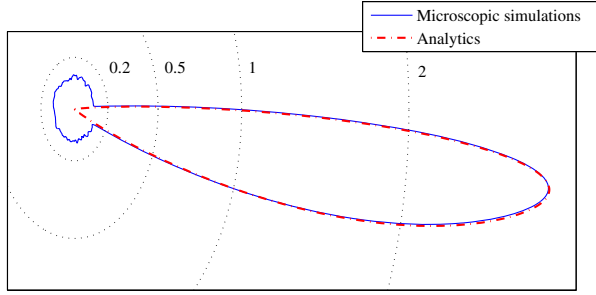


Fig. 2. Radiation pattern of light scattered ($|E|^2$) by an atom cloud under the influence of a differential Zeeman effect. Incident from the left, the light is deflected by a transverse magnetic field gradient. The analytical curve (red dashed) corresponds to Eq. (8), whereas the microscopic curve (blue solid) is obtained from simulations of the stationary solution of Eq. (2). The simulations are made for a cloud of $N = 100$ atoms with radius $\sigma = 35$ ($b_0 = 0.16$) and $\alpha = 1$. The microscopic simulations are averaged over 500 realizations. $|E|^2$ is in arbitrary unit, the dotted contour lines stand for its level.

single-scattering regime, i.e., for low optical thickness $b_0 = 2N/\sigma^2$. Let us remark that the normalized gradient α scales with the transition linewidth Γ , so different transitions may produce very different deviations.

The expansion in scattering orders is also investigated numerically, using Gaussian distributions $\{\mathbf{r}_i\}$ for direct simulations of the microscopic problem. Then, the single-scattering contribution is obtained by considering the single-scattering dipole excitation $\beta_j^{(1)} = (\Omega_0/\Gamma)/(i + 2\Delta(\mathbf{r}_j)/\Gamma)$, from which the radiated field is derived. The following scattering order is obtained as $\beta_j^{(2)} = \sum_m \mathbf{K}_{jm} \beta_m^{(1)}$, where the scattering matrix \mathbf{K} has components $\mathbf{K}_{jm} = K(\mathbf{r}_j, \mathbf{r}_m)$ for $j \neq m$ and $\mathbf{K}_{jj} = 0$. Each higher scattering order is obtained by applying K on the previous one.

An illustration of Eq. (8) exhibiting the lighthouse effect is shown in Fig. 2. It clearly demonstrates how the transverse phase gradient deflects the incoming light. Furthermore, Eq. (8) appears to be in excellent agreement with numerical simulations of the microscopic problem of Eq. (2) realized in a regime where the cloud is optically thin ($b_0 = 0.16$). Indeed, the only difference between the two radiation patterns is an (apart from some noise) isotropic background present in the microscopic simulations. This background has its origin in the atomic disorder, which is naturally absent from our analytical approach.

The deflection angle θ_L is obtained by maximizing Eq. (8) over θ , which leads to

$$\frac{1}{\alpha} - \sigma \sqrt{\frac{2 \exp\left[-\frac{1}{2}\left(\frac{1}{|\alpha|\sigma} + \text{sign}(\alpha)\sigma \sin \theta_L\right)^2\right]}{\pi \operatorname{erfc}\left(\frac{1}{\sqrt{2}}\left(\frac{1}{|\alpha|\sigma} + \text{sign}(\alpha)\sigma \sin \theta_L\right)\right)}} = \sigma^2 \tan \theta_L (1 - \cos \theta_L). \quad (9)$$

Figure 3 compares the calculated deflection angle to microscopic simulations of Eq. (2), confirming the validity of the above formula. Under the approximation of a small total detuning over the cloud ($\alpha\sigma \ll 1$), we get

$$\theta_L = \sin^{-1}\left(\frac{1 - \sqrt{1 + 4\alpha^2\sigma^2}}{2\alpha\sigma^2}\right) \approx -\alpha. \quad (10)$$

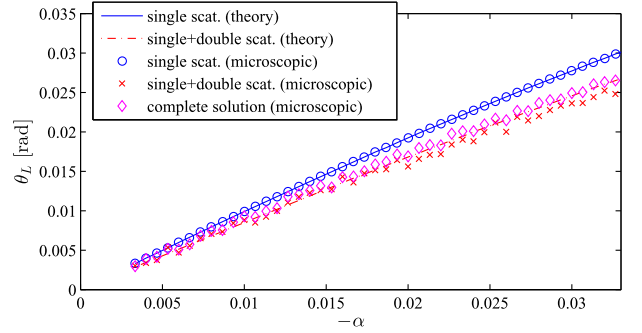


Fig. 3. Deflection angle θ_L as a function of the scaled magnetic field gradient α . The curves correspond respectively to single- (solid blue) and double-scattering (dashed red) contributions. The crosses, plus signs, and squares stand, respectively, for microscopic single-, double-, and full-scattering solutions. The simulations were realized for a cloud with radius $\sigma = 21$ ($b_0 = 0.5$) of $N = 113$ atoms, and averaged over 100 realizations.

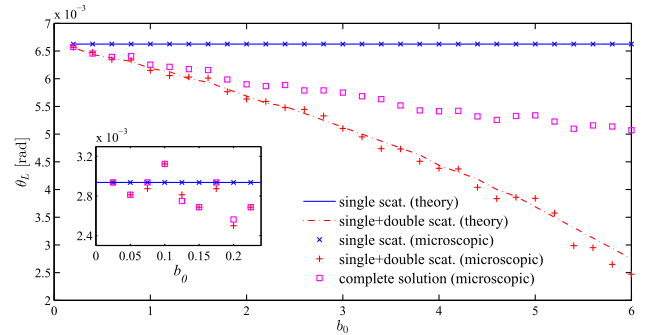


Fig. 4. Deflection angle θ_L as a function of the optical thickness b_0 . The curves correspond respectively to single- (solid blue) and double-scattering (dashed red) contributions. The crosses, plus signs, and squares stand for, respectively, microscopic single-, double-, and full-scattering solutions. Simulations realized for a cloud of radius $\sigma = 21$, varying the number of particles N according to $b_0 = 2N/\sigma^2$, and averaged over 100 realizations. The inset shows the convergence to the single-scattering prediction for vanishing b_0 . The latter simulations were realized for a system size $\sigma = 57$, in order to get sufficient a particle number at low optical thickness.

In the other limit of large α , note that the deviation angle is not limited by the diffraction limit from the cloud size. Indeed, an increasing gradient of the magnetic field means that only a smaller volume of atoms scatter the light efficiently, thus reducing the effective size of the macroscopic scatterer (see Fig. 7).

Yet, as one increases the optical thickness of the cloud (see Fig. 4), the single-scattering prediction loses its accuracy, pointing to the fact that the optically dense regime is ruled by photon rescattering. While an exact solution of the three-dimensional scattering problem including interference does not, to the best of our knowledge, exist, it is possible to probe the dense regime using, for example, a multiple-scattering expansion [19–22]. As we will see now, the double-scattering contribution can be evaluated, providing valuable hints of the dense regime.

4. MULTIPLE-SCATTERING REGIME

An analytical treatment of the multiple-scattering regime involves solving the problem of N fully coupled atom dipoles

[23–25]. Mean-field approaches such as the timed Dicke state [26] (TDS), or random walk approaches neglecting phase coherences, obviously cannot capture the modification of the atomic phase field. We thus resort to a multiple-scattering expansion, an approach that has proved particularly useful in the treatment of, e.g., coherent backscattering [20,27–29].

The double-scattering contribution to the field is obtained in Appendix A as

$$\begin{aligned}
 E^{(2)}(\theta) = & NE_0 \frac{\sqrt{\pi} e^{1/(4\alpha^2\sigma^2) + \sin\theta/(2\alpha) - \sigma^2(1-\cos\theta)^2/4} e^{ik_0 r}}{16|\alpha|\sigma} \frac{1}{r} \\
 & \times \operatorname{erfc}\left(\frac{1}{2|\alpha|\sigma} + \frac{\operatorname{sign}(\alpha)\sigma \sin\theta}{2}\right) \\
 & \times \frac{b_0}{\cos\frac{\theta}{2}} [e^{-\sigma^2(1+\sin\theta)^2} \operatorname{erfc}(-i\sigma(1+\sin\theta)) \\
 & - e^{-\sigma^2(1-\sin\theta)^2} \operatorname{erfc}(-i\sigma(1-\sin\theta))]. \quad (11)
 \end{aligned}$$

In Eq. (11), the first line describes the light deviation, while the second line yields the double-scattering process: the prefactor containing the optical thickness is typical for such an expansion. The validity of this expansion is delimited by the condition $b_0 < 1$, when single- and double-scattering are the dominant contributions.

In Fig. 5, the first-, second-, and complete-scattering solutions for the microscopic problem are plotted and compared to the analytical solution. The single- and double-scattering contributions are correctly predicted by the theory. Furthermore, the figure shows a reduction in the deflection angle as the optical thickness increases. Thus, the rescattering of the light by the atoms tends to erase the dipole phase gradient imposed by the magnetic field.

We note that the single- and double-scattering fields interfere destructively, since their electric fields have opposite signs. Thus, a careful treatment of the light field amplitude rather than the intensity is crucial, as already noted in [22].

As the optical thickness increases beyond unity, the numerical full-scattering solution, which contains all scattering orders, deviates from the prediction obtained for double-scattering. This is confirmed by the analysis performed in Fig. 4, where the deviation angle appears correctly predicted by the single-scattering approach for $b_0 \ll 1$ and by the double-scattering calculations for $b_0 \leq 1$. The extremum equation for the deflection angle θ_L including double-scattering is straightforwardly derived from Eq. (11), yet cumbersome, for which reason it is not presented here.

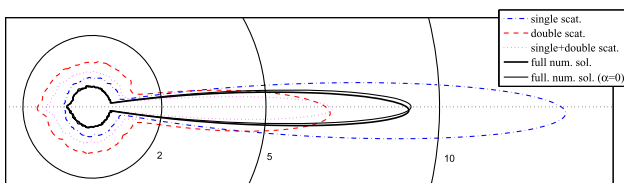


Fig. 5. Radiation pattern $|E|^2$ for different scattering orders (see legend), for the microscopic system. The solid thick and thin lines correspond respectively to the numerical full-scattering solution with and without the gradient of the magnetic field. Simulations realized for a cloud of $N = 225$ atoms, $\sigma = 21$ ($b_0 = 1$), and $\alpha = 0.013$, and averaged over 500 configurations. $|E|^2$ is in arbitrary units, the solid contour lines stand for its level.

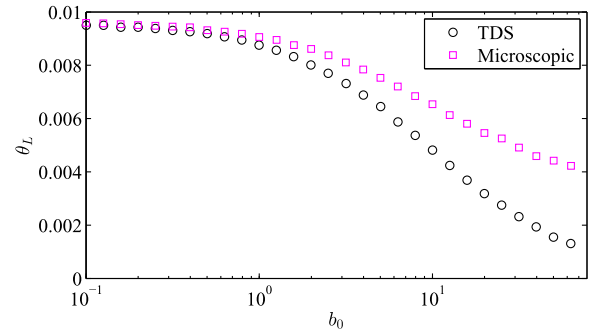


Fig. 6. Deviation angle for optically thick samples. Simulations realized for a cloud of size $\sigma = 21$, the number of particles being determined by the optical thickness, and $\alpha = -0.01$. The timed Dicke state (TDS) symbols refer to single-scattering calculations using the collective linewidth.

Features of the deep multiple-scattering regime can be captured using a modified timed Dicke state: this mean-field ansatz assumes a perfect synchronization of all atomic dipoles [26] and, as a consequence, a broadening of the atomic linewidth. For a Gaussian cloud, the collective linewidth is $\Gamma_N = \Gamma(1 + b_0/8)$ [30]. In our case, we also need to account for an effective reduction in the optical thickness due to the inhomogeneous detuning imposed by the gradient of the magnetic field. The average detuning of the atoms compared to those on the optical axis being $\delta_{\text{LH}} = \alpha\sigma$, the effective optical thickness for the cloud is $b^{\text{eff}} = b_0/(1 + 4\delta_{\text{LH}}^2)$.

Replacing the atomic linewidth by the collective one $\Gamma(1 + b^{\text{eff}}/8)$ in the single-scattering prediction, we predict a reduction in the lighthouse effect as the optical density increases: the increase in linewidth leads to a decrease in the normalized gradient α . Simulations of the microscopic problem confirm that result and show a qualitative agreement with the prediction of the modified timed Dicke ansatz (see Fig. 6).

5. DISCUSSION AND EXPERIMENTAL PERSPECTIVES

We investigated the deflection of light by an atomic cloud under the influence of a differential Zeeman shift and found that the single-scattering regime yields maximum deflection. Calculations and simulations for clouds of larger optical density, which are dominated by multiple scattering, revealed a reduction in the effect. This observation points to the fact that the lighthouse deflection is clearly not a cooperative effect in the sense that it does not result from light-mediated interaction of the atoms. It is rather similar to Bragg scattering, where the scattering pattern generated by the interference of the radiated waves provides information about the atomic cloud's structure. As soon as the atoms interact through their radiation, the emergence of multiple scattering washes out the phase gradient imposed externally by the magnetic field.

Our predictions can be experimentally verified, e.g., with a cloud of spatially confined cold atoms exposed to a uniform magnetic field gradient. Measurable deflections are expected when the parameter α is not too small compared to 1. According to the definition of α [below Eq. (7)], for a typical magnetic field gradient of $\eta = 100$ G/cm, this requires rather small linewidths of the atomic transition. A possible system would be a cloud of ultracold strontium driven on its intercombination line at $\lambda = 2\pi/k = 689$ nm. The transition linewidth being

$\Gamma = (2\pi)7.6$ kHz one could reach $\alpha = 0.8$ with the specified gradient.

In our derivations we assumed a single excited state Zeeman level. However, if the atomic cloud is trapped in a magneto-optical trap (MOT) we would rather have a distribution of atoms in all Zeeman levels. Furthermore, the magnetic field does not have the geometry of a uniform gradient but of a quadrupolar field. These problems, can, however, be circumvented by suddenly applying a magnetic field offset B_0 and simultaneously detuning the probe light beam to the Zeeman-shifted resonance. In that way, one spectrally filters out a single Zeeman state, i.e., the probe light predominantly interacts with atoms occupying a single Zeeman level. This requires $B_0 \gg \Gamma$, which is easy to satisfy in the case of a narrow linewidth Γ .

Typical values for a strontium MOT operated on the narrow intercombination line are an atom number of $N = 2 \cdot 10^7$ and a radial size of $\bar{R} = 70 \mu\text{m}$ (or $\sigma = k\bar{R} \simeq 640$) [31], giving an optical density of $b_0 = 2N/(k\bar{R})^2 \simeq 100$ for the intercombination line. In practice, however, narrow transitions are generally dominated by Doppler broadening. At a temperature of $4 \mu\text{K}$, for example, the Doppler broadening of the intercombination line is $k\bar{v} = k\sqrt{k_B T/m} = (2\pi) 28$ kHz. Even if the temperature is at the Doppler limit of the intercombination line, $T_D = \hbar\Gamma/k_B = 365$ nK, the Doppler width still is 8.5 kHz.

To prevent blurring of the lighthouse deflection by the thermal atomic motion, it is important that the Doppler shift be smaller than the Zeeman shift, $k\bar{v} \ll \bar{R}\partial_\delta B$. In this case, the main effect of the thermal motion is to reduce the optical thickness of the atomic cloud, by a factor corresponding to the spectral overlap between the natural linewidth and the Doppler broadened width, $b_D = b_0\Gamma/kv$.

Another point ruling the detectability of the lighthouse deflection is, whether it exceeds the probe beam divergence angle. Assuming that it is optimally matched to the size of the cloud, $w_0 = \bar{R} = 70 \mu\text{m}$, we obtain the divergence angle $\alpha_{\text{div}} = \lambda/\pi w_0 = 0.18^\circ$. Since $\sigma = 70 \mu\text{m}/689 \text{ nm} \approx 101$ and $\alpha \approx 0.4$, the deflection angle predicted by Eq. (9) is $\theta_L = 1.34^\circ$,

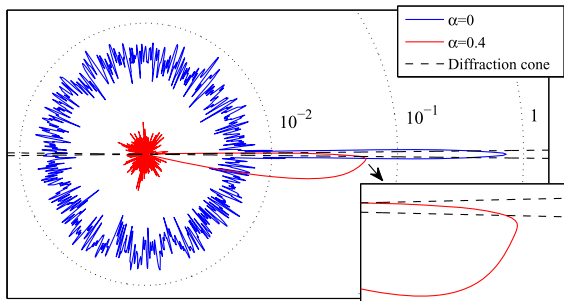


Fig. 7. Radiation pattern normalized by the incident intensity $|E/E_0|^2$ for the microscopic system, with (thick red) and without (thin blue) the gradient of the magnetic field. The inset allows us to observe that the lighthouse angle is not diffraction-limited (cone of black dashed lines; see main text). Note that the strong background radiation is due to the limited number of particles that can be simulated. The reduced radiated intensity in the presence of the gradient of the magnetic field is due to the fact that many atoms are driven out of resonance by it, so their coupling with the light is reduced. Simulations realized for a cloud of $N = 15000$ atoms, $\sigma = 101$ ($b_0 = 2.94$) and $\alpha = 0.4$, and averaged over 10 configurations. $|E|^2$ is in arbitrary units, the dotted contour lines stand for its level.

so that the deviated beam is easily separated from the incident laser (see Fig. 7).

Even on regular MOTs operating on strong transitions, the atomic lighthouse effect should be detectable. Considering, for instance, the broad $^1S_0 - ^1P_1$ transition in strontium [$\Gamma = (2\pi)32$ MHz], we estimate a deflection angle of $\theta_L = 0.026^\circ$, which is of the same order of magnitude as the divergence angle, which for a MOT radius of typically $\bar{R} = 3$ mm, would be $\alpha_{\text{div}} = 0.028^\circ$.

The experimental verification of the lighthouse effect would represent a nice confirmation that our actual understanding of how light is cooperatively scattered by ensembles of particles is correct, as the reduction in the deviation angle provides a direct measure of the collective atomic linewidth.

APPENDIX A: SINGLE- AND DOUBLE-SCATTERING STRUCTURE FACTOR

In the far-field limit and at a distance r , the single-scattering field is given by

$$E^{(1)}(\mathbf{k}) = -\frac{NE_0}{(2\pi)^3 R^3} \frac{e^{ik_0 r}}{r} \int_{-\infty}^{\infty} e^{i(1-\cos\theta)k_0 z} e^{-z^2/2R^2} dz \\ \times \int_{-\infty}^{\infty} e^{-ik_0 y \sin\theta} \sin\phi e^{-y^2/2R^2} dy \\ \times \int_{-\infty}^{\infty} \frac{e^{-ik_0 x \sin\theta \cos\phi} e^{-x^2/2R^2}}{1 - iak_0 x} dx.$$

The first integral gives $\exp(-(1-\cos\theta)^2\sigma^2/2)$ that yields the forward emission of Rayleigh scattering, in a cone of width $\sim 1/\sigma$. The second integral produces a $\exp(-\sin^2\theta \sin^2\phi\sigma^2/2)$, yet since the problem is symmetric with respect to the (\hat{x}, \hat{z}) plane, we restrict ourselves to this plane, taking $\phi = 0, \pi$. Finally, the integral over x , that contains the deviation is

$$\int_{-\infty}^{\infty} \frac{e^{\pm ik_0 x \sin\theta} e^{-x^2/2R^2}}{1 - iak_0 x} dx = \gamma^2 \int_{-\infty}^{\infty} e^{-x^2/2R^2} \cos ax \frac{dx}{\gamma^2 + x^2} \\ \pm \text{sign}(\gamma) |\gamma| \int_{-\infty}^{\infty} e^{-x^2/2R^2} \sin ax \frac{x dx}{\gamma^2 + x^2},$$

with $a = k_0 \sin\theta$ and $\gamma = 1/ak_0$, and where the \pm signs refer to the cases $\phi = 0, \pi$. Both integrals are solved using integral formula [32]

$$\int_{-\infty}^{\infty} e^{-x^2/2R^2} \sin ax \frac{x dx}{\gamma^2 + x^2} = -\frac{\pi}{2} e^{\gamma^2/2R^2} \left[e^{a|\gamma|} \text{erfc}\left(\frac{1}{\sqrt{2}}\left(\frac{|\gamma|}{R} + aR\right)\right) - e^{-a|\gamma|} \text{erfc}\left(\frac{1}{\sqrt{2}}\left(\frac{|\gamma|}{R} - aR\right)\right) \right], \quad (\text{A1})$$

$$\int_{-\infty}^{\infty} e^{-x^2/2R^2} \cos ax \frac{dx}{\gamma^2 + x^2} = \frac{\pi}{2|\gamma|} e^{\gamma^2/2R^2} \left[e^{-a|\gamma|} \text{erfc}\left(\frac{1}{\sqrt{2}}\left(\frac{|\gamma|}{R} - aR\right)\right) + e^{a|\gamma|} \text{erfc}\left(\frac{1}{\sqrt{2}}\left(\frac{|\gamma|}{R} + aR\right)\right) \right]. \quad (\text{A2})$$

Consequently, we have

$$\int_{-\infty}^{\infty} \frac{e^{\pm i \sin \theta k_0 x} e^{-x^2/2R^2}}{1 - iak_0 x} dx = \pi |\gamma| e^{\frac{\gamma^2}{2R^2}} e^{\pm \text{sign}(\gamma)a|\gamma|} \times \text{Erfc} \left[\frac{1}{\sqrt{2}} \left(\frac{|\gamma|}{R_x} \pm \text{sign}(\gamma)aR_x \right) \right].$$

This leads to Eq. (8), since the \pm can be replaced by $+$ by extending the angle range to interval $0 \leq \theta \leq 2\pi$.

The double-scattering field is given by the expression

$$E^{(2)}(\mathbf{k}) = \frac{\hbar\Gamma}{id} \frac{e^{ik_0 r}}{r} \int d^3\mathbf{r}\rho(\mathbf{r})e^{-ik\cdot\mathbf{r}} \int d^3\mathbf{r}'\rho(\mathbf{r}')K(\mathbf{r},\mathbf{r}')\beta^{(1)}(\mathbf{r}'). \quad (\text{A3})$$

These integrals can be decoupled for a Gaussian density distribution, using the following change of variables

$$\mathbf{u} = \frac{\mathbf{r} - \mathbf{r}'}{\sqrt{2}}, \quad \mathbf{w} = \frac{\mathbf{r} + \mathbf{r}'}{\sqrt{2}}, \quad (\text{A4})$$

so that $\rho(\mathbf{r})\rho(\mathbf{r}') = \rho(\mathbf{u})\rho(\mathbf{w})$, and assuming that the quadratic terms in w^2 and v^2 can be neglected in the Zeeman term (approximation of small frequency shift $2\alpha^2\sigma^2 \ll 1$). Then we obtain

$$E^{(2)}(\mathbf{k}) = E_0 \frac{e^{ik_0 r}}{r} \int d^3\mathbf{u}\rho(u) \frac{e^{i\sqrt{2}u}}{i\sqrt{2}u} e^{-i\mathbf{u}\cdot(\mathbf{k}_0+\mathbf{k})/\sqrt{2}} \times \int \frac{d^3\mathbf{w}\rho(w)e^{i\mathbf{w}\cdot(\mathbf{k}_0-\mathbf{k})/\sqrt{2}}}{1 + i\sqrt{2}\alpha\mathbf{w}\cdot\hat{x}}. \quad (\text{A5})$$

Similar to the single-scattering case, the second integral I_w in Eq. (A5) leads to

$$I_w(\theta) = \frac{\sqrt{\pi}}{2} \frac{N}{|\alpha|\sigma} \exp\left(\frac{1}{4\alpha^2\sigma^2} + \frac{\text{sign}(\alpha)\sin\theta}{2|\alpha|} - \frac{\sigma^2}{4}(1 - \cos\theta)^2\right) \times \text{erfc}\left(\frac{1}{2}\left(\frac{1}{|\alpha|\sigma} + \text{sign}(\alpha)\sigma\sin\theta\right)\right). \quad (\text{A6})$$

The first integral, I_u , in Eq. (A5) is calculated using spherical coordinates (u, θ_u, ϕ_u) . The integral over ϕ_u leads to

$$\begin{aligned} I_u(\theta) &= \frac{N}{i2\sqrt{\pi}k_0R^3} \int_0^\infty u e^{-u^2/2R^2 + i\sqrt{2}k_0u} du \int_0^\pi \sin\theta_u e^{-i\frac{k_0u}{\sqrt{2}}(1+\cos\theta)\cos\theta_u} J_0\left(\frac{k_0u\sin\theta\sin\theta_u}{\sqrt{2}}\right) d\theta_u \\ &= \frac{N}{i\sqrt{2\pi}k_0^2R^3 \cos\frac{\theta}{2}} \int_0^\infty e^{-u^2/2R^2 + i\sqrt{2}k_0u} \sin\left(\sqrt{2}k_0u\cos\frac{\theta}{2}\right) du \\ &= -\frac{b_0}{8\cos\frac{\theta}{2}} \left[\exp\left(-\sigma^2\left(1 + \cos\frac{\theta}{2}\right)^2\right) \times \text{erfc}\left(-i\sigma\left(1 + \cos\frac{\theta}{2}\right)\right) - \exp\left(-\sigma^2\left(1 - \cos\frac{\theta}{2}\right)^2\right) \times \text{erfc}\left(-i\sigma\left(1 - \cos\frac{\theta}{2}\right)\right) \right], \quad (\text{A7}) \end{aligned}$$

where we have introduced the optical thickness $b_0 = 2N/\sigma^2$.

ACKNOWLEDGMENTS

We acknowledge financial support from IRSES project COSCALI, from USP/COFECUB (projet Uc Ph 123/11), and from GDR “Nanomagnetism, Spin Electronics, Quantum Optics, and Quantum Technologies.” C. E. M., Ph. W. C., and R. B. acknowledge support from the Brazilian FAPESP and CNPq agencies.

REFERENCES

1. R. H. Dicke, “Coherence in spontaneous radiation processes,” *Phys. Rev.* **93**, 99–110 (1954).
2. R. Friedberg, S. R. Hartmann, and J. T. Manassah, “Frequency shifts in emission and absorption by resonant systems of two-level Atoms,” *Phys. Rep. C* **7**, 101179 (1973).
3. R. Röhlsberger, K. Schlage, B. Sahoo, S. Couet, and R. Ruffer, “Collective lamb shift in single-photon superradiance,” *Science* **328**, 1248–1251 (2010).
4. J. Keaveney, A. Sargsyan, U. Krohn, I. G. Hughes, D. Sarkisyan, and C. S. Adams, “Cooperative lamb shift in an atomic vapor layer of nanometer thickness,” *Phys. Rev. Lett.* **108**, 173601 (2012).
5. I. H. Deutsch, R. J. C. Spreeuw, S. L. Rolston, and W. D. Phillips, “Photonic band gaps in optical lattices,” *Phys. Rev. A* **52**, 1394–1410 (1995).
6. M. Antezza and Y. Castin, “Fano–Hopeld model and photonic band gaps for an arbitrary atomic lattice,” *Phys. Rev. A* **80**, 013816 (2009).
7. A. Schilke, C. Zimmermann, P. Courteille, and W. Guerin, “Photonic band gaps in one-dimensionally ordered cold atomic vapors,” *Phys. Rev. Lett.* **106**, 223903 (2011).
8. M. Antezza and Y. Castin, “Photonic band gap in an imperfect atomic diamond lattice: penetration depth and effects of finite size and vacancies,” *Phys. Rev. A* **88**, 033844 (2013).
9. M. Samoylova, N. Piovella, R. Bachelard, and P. Courteille, “Microscopic theory of photonic bandgaps in optical lattices,” *Opt. Commun.* **312**, 94–98 (2014).
10. R. Röhlsberger, T. S. Toellner, W. Sturhahn, K. Quast, E. E. Alp, A. Bernhard, E. Burkel, O. Leupold, and E. Gerdau, “Coherent resonant x-ray scattering from a rotating medium,” *Phys. Rev. Lett.* **84**, 1007–1010 (2000).
11. R. Röhlsberger, T. Toellner, K. Quast, W. Sturhahn, E. Alp, and E. Burkel, “The nuclear lighthouse effect: a new tool for high-resolution X-ray spectroscopy,” *Nucl. Instrum. Methods Phys. Res. Sect. A* **467–468**, 1473–1476 (2001).
12. R. Röhlsberger, K. Quast, T. S. Toellner, P. L. Lee, W. Sturhahn, E. E. Alp, and E. Burkel, “Observation of the 22.5-keV resonance in $(149)\text{Sm}$ by the nuclear lighthouse effect,” *Phys. Rev. Lett.* **87**, 047601 (2001).
13. T. Roth, O. Leupold, H.-C. Wille, R. Ruffer, K. W. Quast, R. Röhlsberger, and E. Burkel, “Coherent nuclear resonant scattering by $(61)\text{Ni}$ using the nuclear lighthouse effect,” *Phys. Rev. B* **71**, 140401(R) (2005).
14. L. Karpa and M. Weitz, “A Stern–Gerlach experiment for slow light,” *Nat. Phys.* **2**, 332–335 (2006).
15. L. Karpa and M. Weitz, “Nondispersive optics using storage of light,” *Phys. Rev. A* **81**, 041802 (2010).
16. U. Schnorrberger, J. D. Thompson, S. Trotzky, R. Pugatch, N. Davidson, S. Kuhr, and I. Bloch, “Electromagnetically induced transparency and light storage in an atomic Mott insulator,” *Phys. Rev. Lett.* **103**, 033003 (2009).
17. V. A. Sautenkov, H. Li, Y. V. Rostovtsev, and M. O. Scully, “Ultra-dispersive adaptive prism based on a coherently prepared atomic medium,” *Phys. Rev. A* **81**, 063824 (2010).
18. T. Bienaime, M. Petruzzo, D. Bigerni, N. Piovella, and R. Kaiser, “Atom and photon measurement in cooperative scattering by cold atoms,” *J. Mod. Opt.* **58**, 1942–1950 (2011).
19. A. Ishimaru, *Wave Propagation and Scattering in Random Media* (Academic, 1978), Vol 2.
20. M. B. van der Mark, M. P. van Albada, and A. Lagendijk, “Light scattering in strongly scattering media: multiple scattering and weak localization,” *Phys. Rev. B* **37**, 3575–3592 (1988).

21. T. M. Nieuwenhuizen, A. Lagendijk, and B. A. van Tiggelen, "Resonant point scatterers in multiple scattering of classical waves," *Phys. Lett. A* **169**, 191–194 (1992).
22. M.-T. Rouabah, M. Samoylova, R. Bachelard, P. W. Courteille, R. Kaiser, and N. Piovella, "Coherence effects in scattering order expansion of light by atomic clouds," *J. Opt. Soc. Am. A* **31**, 1031–1039 (2014).
23. M. Chalony, R. Pierrat, D. Delande, and D. Wilkowski, "Coherent flash of light emitted by a cold atomic cloud," *Phys. Rev. A* **84**, 011401R (2011).
24. S. E. Skipetrov and I. M. Sokolov, "Absence of Anderson localization of light in a random ensemble of point scatterers," *Phys. Rev. Lett.* **112**, 023905 (2014).
25. J. Pellegrino, R. Bourgain, S. Jennewein, Y. R. P. Sortais, S. D. Jenkins, J. Ruostekoski, and A. Browaeys, "Observation of suppression of light scattering induced by dipole-dipole interactions in a cold atomic ensemble," arXiv:1402.4167 (2014).
26. M. Scully, E. Fry, C. Ooi, and K. Wodkiewicz, "Directed spontaneous emission from an extended ensemble of N atoms: timing is everything," *Phys. Rev. Lett.* **96**, 010501 (2006).
27. E. Akkermans, P. E. Wolf, and R. Maynard, "Coherent backscattering of light by disordered media: analysis of the peak line shape," *Phys. Rev. Lett.* **56**, 1471–1474 (1986).
28. P.-E. Wolf and G. Maret, "Weak localization and coherent backscattering of photons in disordered media," *Phys. Rev. Lett.* **55**, 2696 (1985).
29. M. P. V. Albada and A. Lagendijk, "Observation of weak localization of light in a random medium," *Phys. Rev. Lett.* **55**, 2692–2699 (1985).
30. P. W. Courteille, S. Bux, E. Lucioni, K. Lauber, T. Bienaim, R. Kaiser, and N. Piovella, "Modification of radiation pressure due to cooperative scattering of light," *Eur. Phys. J. D* **58**, 69–73 (2010).
31. T. Chanélière, D. Wilkowski, Y. Bidet, R. Kaiser, and C. Miniatura, "Saturation-induced coherence loss in coherent backscattering of light," *Phys. Rev. E* **70**, 036602 (2004).
32. I. S. Gradshteyn and I. M. Ryzhik, *Table of Integrals, Series, and Products*, 7th ed. (Elsevier/Academic, 2007).